Electrochemistry
The Electrochemical Society of Japan
Received: December 21, 2023
Accepted: January 14, 2024
Published online: January 17, 2024
Issued: April 1, 2024
https://doi.org/10.5796/electrochemistry.23-69151
Article
Electrochemistry, **92(4)**, 043011 (2024)

The 69th special feature "Frontiers of Molten Salts and Ionic Liquids"

Arrangement of Al Ions between Ionic Liquid and Graphite Electrode Interface by AFM Force Curve Measurement†

Atsuki TABO,[a] Hisayoshi MATSUSHIMA,[a,§] Takahiro OHKUBO,[b,§] Kei NISHIKAWA,[b,c,§] and Mikito UEDA[a,*,§]

[a] *Graduate School of Engineering, Hokkaido University, Kita-13, Nishi-8, Kita-ku, Sapporo, Hokkaido 060-8628, Japan*
[b] *Graduate School of Engineering, Chiba University, 1-33 Yayoi-cho, Inage-ku, Chiba 263-8522, Japan*
[c] *National Institute of Materials Science (NIMS), 1-1 Namiki, Tsukuba, Ibaraki 305-0044, Japan*

* *Corresponding author: mikito@eng.hokudai.ac.jp*

ABSTRACT

The arrangement of ions at the interface between highly oriented pyrolytic graphite (HOPG) and Aluminum chloride–1-ehtyl-3-methylimidazolium chloride ($AlCl_3$–EmImCl) ionic liquid was evaluated using Atomic Force Microscopy (AFM) force curve measurements. In the force curve measurements, three steps were observed towards the HOPG electrode. The width of each step was 0.3, 0.4, and 0.5 nm in order from the final arrival point. Their step widths were regarded as the thicknesses of $EmIm^+$, $Al_2Cl_7^-$, or their mixed layers. The force curve measurements at each potential demonstrated that the width of the first layer close to the HOPG tended to decrease as the potential shifted towards the less noble side.

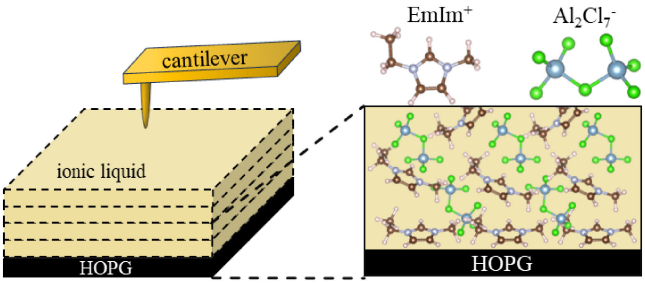

Keywords : Ionic Liquid, AFM Force Curve Measurement, Ion Arrangement

1. Introduction

Ionic liquids and molten salts are liquids composed only of ions and have high thermal stability, wide electrical window, and high electrical conductivity. Because of these characteristics, ionic liquids are used in various electrochemistry fields, such as the electrodeposition of metals and electrolytes for batteries.[1–5] To understand the phenomena or electrode reaction in electrochemistry, it is important to understand the structure of the solid-liquid interface. The widely known model for the electrode-electrolyte interface in aqueous solution is the Gouy-Chapman-Stern (GCS) model of the electric double layer.[6] Unlike aqueous solutions, ionic liquids do not contain neutral liquids like water, thus it is difficult to apply this model. Fedorov et al. reported a model of the interface[7] for the bias of ions near the interface of ionic liquids, and Mezger et al. experimentally confirmed the formation of layers of fluorinated ionic liquids at the charged sapphire interface by high-energy X-ray reflectometry.[8] A rough model of the ionic species structure at the electrode interface has also established from the results of the same paper and simulation studies by Martin et al.[9] and Ivaništšev et al.[10] When the electrode is positively charged, the anions are arranged on the surface, followed by cations in the next layer, and gradually a mixed layer of anions and cations is formed, leading to the bulk; a schematic illustration of each layer is shown in Fig. 1. The current structure of the interface at the ionic liquid/electrode has also been proposed from in-situ observations by spectroscopy[11] and Scanning Tunneling Microscope,[12] and the presence of arranged layers of ions different from the bulk has been reported. A commonly used technique in the study of the solid/liquid interface of ionic liquids is AFM, which is an experimental technique for imaging surface structures using a small probe cantilever. Fukui reported detailed imaging of ionic structures at electrode interfaces using Frequency Modulation-Atomic Force Microscopy (FM-AFM).[13]

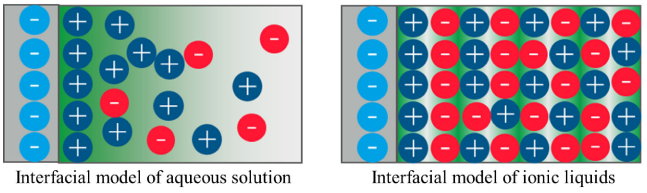

Figure 1. Schematic diagram of the electrode interface and ionic array in aqueous solution/ionic liquid.

In studies using AFM measurements, it is possible to measure the thickness of the ionic layer and the penetration intensity through that layer from the force curve measurements as well as imaging. In force curve measurements, the cantilever is brought close to the electrode surface, and when it reaches a certain distance, the cantilever is pulled back. It is then deflected by the attractive/

†The contents include the authors' presentation #P45 at 2023 Joint Symposium on Molten Salts (MS12).
§ECSJ Active Member
M. Ueda orcid.org/0000-0003-2068-1715

repulsive forces generated by the sample surface. The adsorption force and elasticity of the surface can be measured based on this AFM deflection.

Rob Atkin et al. evaluated the ion layer thickness, layer strength, and number of arranged ion layers of 1-butyl-1-methylpyrrolidinium tris(pentafluoroethyl) trifluorophosphate ([Py1,4][FAP]), 1-ethyl-3-methylimidazolium tris(perfluoroethyl)trifluorophosphate ([EmIm][FAP]), 1-Ethyl-3-methylimidazolium Bis(trifluoromethanesulfonyl)imide ([EmIm][TFSA]), and 1-butyl-1-methylpyrrolidinium bis[(trifluoromethyl)sulfonyl]amide ([BMP][TFSA]) on the gold substrate surface.[14,15] Fukui et al. reported on the magnitude of the force required to penetrate the solvation layer at the ionic liquid/rubrene single crystal interface by force curve measurements.[16] In this technique, the cantilever penetrates the ionic layer formed at the interface, resulting in a change in the graph as it approaches the interface. In addition, a force change occurs when the cantilever penetrates the ionic layer formed at the interface and reaches the next ionic layer. This change is observed as a step, rather than the gentle curve it was before. Subsequently, the width of the ion layer and the force required to penetrate it are measured. Cantilevers are change-sensitive probes and are therefore suitable for capturing changes in objects such as ionic layers, which can be altered by minute forces. Changes in the ionic layer at the interface of ionic liquids depend on the constituent ionic species, but also occur when an electric field is applied. The application of electric fields to ionic liquids has been conducted in the studies of solvents[17] and lubricants[18] in the field of energy storage, such as batteries and capacitors.[19–21] The AFM force curve measurement used in this experiment allows in-situ observation while applying an electric potential.

Ionic liquids are also expected to be applied as electrolytes in electroplating.[22,23] A typical example is aluminum electroplating, in which many reports are of ionic liquids made by mixing 1-ehtyl-3-methylimidazolium chloride (EmImCl) and Aluminium chloride ($AlCl_3$). The ionic liquid is in a liquid state near 25 °C, which enables aluminum plating on low-melting-point substrate materials. In the $AlCl_3$–EmImCl ionic liquid, the reaction of Eq. 1 proceeds.[24]

$$AlCl_3 + EmImCl \rightarrow AlCl_4^- + EmIm^+ \quad (1)$$

Furthermore, the addition of excess $AlCl_3$ generates the dimeric complex ion of aluminum shown in Eq. 2.

$$AlCl_4^- + AlCl_3 \rightarrow Al_2Cl_7^- \quad (2)$$

$Al_2Cl_7^-$ in this ionic liquid are electrodeposited as metallic aluminum at the cathode in the reaction of Eq. 3.[24]

$$4Al_2Cl_7^- + 3e^- \rightarrow Al + 7AlCl_4^- \quad (3)$$

The electrical conductivity and activity of ionic species in the $AlCl_3$–EmImCl ionic liquid depend on the concentration of $AlCl_3$. In aluminum electrodeposition, the ion required for Al electrodeposition is $Al_2Cl_7^-$ and this ionic species is formed at $AlCl_3$ concentrations above 50 mol%. As reported by R. J. Gale et al. $AlCl_4^-$ decreases and $Al_2Cl_7^-$ concentration increases as the concentration of $AlCl_3$ in the ionic liquid becomes above 50 mol%, and at 67 mol% the Al ionic species alone can be treated as $Al_2Cl_7^-$.[25] Thus, the activity of $Al_2Cl_7^-$ is about 1 at an $AlCl_3$ concentration of 67 mol%, and this composition is commonly used in Al electrodeposition. In the 2 : 1 molar ratio $AlCl_3$–EmImCl ionic liquid used in this experiment, only $EmIm^+$ and $Al_2Cl_7^-$ ions are present, so the $AlCl_3$–EmImCl ionic liquid is denoted [EmIm][Al_2Cl_7] in the following.

The reaction Eq. 3 shows that in the electrodeposition of aluminum, $Al_2Cl_7^-$ receives an electron at the cathode; it remains unclear how $Al_2Cl_7^-$ is reduced by receiving an electron while $EmIm^+$ is present close to the cathode. The authors hope to obtain the AFM force curves with and without an applied electric field to understand the behavior of $Al_2Cl_7^-$ during electrodeposition.

Based on previously reported AFM force curve measurements,[14,15] this study uses force curve measurements at the interface between highly oriented pyrolytic graphite (HOPG) and [EmIm][Al_2Cl_7] ionic liquid to evaluate the process of $Al_2Cl_7^-$ reduction based on the arrangement of layers of ions at the interface and whether a potential is applied.

2. Experimental

Powdered anhydrous aluminum chloride $AlCl_3$ (Kishida Chemical Co., Ltd.) and 1-ethyl-3-methylimidazolium chloride (EmImCl; Tokyo Kasei Kogyo Co., Ltd.) were mixed at a molar ratio of 2 : 1 with cooling. The electrolyte preparation was performed in a glove box with an Ar atmosphere.

After preparation of the ionic liquid, aluminum wires (99.99 %, ϕ 1.5 mm, High Purity Science Laboratory) were immersed in the ionic liquid to remove water and impurities from the ionic liquid and heated to 60 °C for at least seven days.

Furthermore, to remove water from the ionic liquid, pre-electrolysis was carried out at 10 mA for more than 3 h using an Al plate (99.99 %, High Purity Science Laboratory) as the anode and a glassy carbon plate (GC-20, Tokai carbon Co., Ltd.) as the cathode.

Open circuit potential (OCP) and voltammogram measurements were performed in a drying room with a room temperature of 22 °C and a dew point of −60 °C.

The experimental cell shown in Fig. 2 was used for the electrochemical measurements and AFM observations. A HOPG plate (7 × 7 mm) (ALLIANCE Biosystems) was used as the working electrode, a Pt plate as the counter electrode, and an Al wire as the reference electrode. The HOPG plate was bonded to the copper wire by silver paste. The surfaces of the silver paste and copper wire were coated with epoxy adhesive to avoid contact with the ionic liquid electrolyte. A potentiostat (HZ-7000, Meiden Hokuto Corporation) was connected to the cell for the electrochemical measurements. Voltammogram measurements were performed at 22 °C, in the potential range from −0.5 V to 0.5 V (vs. Al/Al(III)), and at a sweep rate of 20 mV s^{-1}.

An AFM (SPM-9700HT, Shimadzu Corporation) was used for the AFM measurements. The cantilever was a NANOSENSORS product with a spring constant of 0.2 N m^{-1}. The force curve measurements were performed at a pushing speed of 20 nm s^{-1}. The measurements were obtained at room temperature. The force curve measurements were performed at open circuit potential. After measurement at open circuit potential, measurements were performed in the chronoamperometry (CA) mode while applying potentials in the range from 0 to 710 mV.

The ion sizes of $EmIm^+$ and $Al_2Cl_7^-$, the target of this experiment, were considered by computer simulation. The optimized geometry of $EmIm^+$ and $Al_2Cl_7^-$ was determined using the DFT/B3LYP/6-311++G(2d,p) level of theory with the Gaussian16

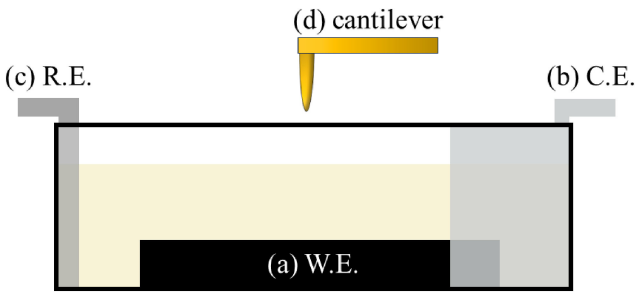

Figure 2. Cross-sectional schematic view of electrochemical cell; (a) HOPG working electrode, (b) Al counter electrode, (c) Al reference electrode, (d) Cantilever.

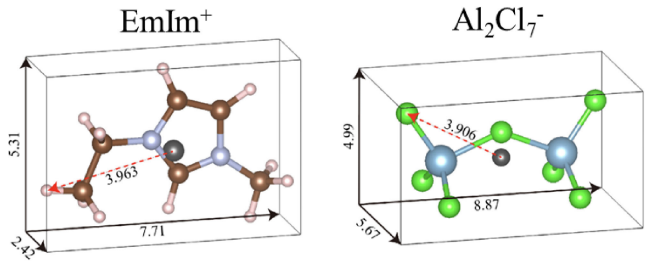

Figure 3. The optimized ionic structure is depicted (left) $EmIm^+$ and (right) $Al_2Cl_7^-$. Black lines along with length in Å are the box edges surround the ions in the standard coordinate system considering the covalent bond radii of the atoms. The red dotted line indicates the distance of the farthest atom from the centroid. The ions are represented by colored balls and sticks (Cl; light green, Al; silver, N; light purple, C; brown, H; white). The centroid position is indicated by a black ball.

package.[26] The centroid for each ion was calculated based on atomic mass and coordinates, utilizing the standard orientation obtained from Gaussian16 output, as depicted in Fig. 3. To gauge the size of the ion, the distance to the farthest atom from the centroid was computed. The lengths of the edges in each axis direction for the standard coordinate system were also calculated to provide information about the degree of anisotropic form.

The dimensions of the cuboid box were derived by considering covalent bond radii (H: 0.32 and Cl: 0.99 in Å). Consequently, the distance from the position of the end atom to the face of the cuboid box was established to be equivalent to the covalent bond radius.

The distances to the farthest atom from the centroid were determined to be 3.963 Å for $EmIm^+$ and 3.906 Å for $Al_2Cl_7^-$. In terms of the cuboid box dimensions, the side lengths for $EmIm^+$ and $Al_2Cl_7^-$ were (7.71, 5.31, 2.42) and (8.87, 5.67, 4.99) in Å for $EmIm^+$ and $Al_2Cl_7^-$ in descending order. The computer-simulated sizes of $EmIm^+$ and $Al_2Cl_7^-$ ions are also shown in Fig. 3 as supporting data for discussion of the experimental results.

3. Results and Discussion

3.1 Electrochemical measurement

The results of the OCP measurements made in the cell in Fig. 2 are shown in Fig. 4. The results show that the OCP was 620 mV vs. Al/Al(III). This potential is considered to be due to the adsorption of a small amount of water in the ionic liquid on the HOPG electrode. The results of the voltammogram measurements are shown in Fig. 4b. The cathode current increased linearly from −100 mV and decreased linearly after reversing the potential, followed by the anode current. These currents correspond to the aluminum electrodeposition reaction and the dissolution reaction of the electrodeposited aluminum, respectively. Because the force curve measurements have to be obtained before the electrodeposition reaction takes place, the potential on the low side was limited to 0 V in this experiment.

3.2 Force curve measurements

The measured results of the force curve at OCP are shown in Fig. 5a. Figure 5b is an enlarged view of Fig. 5a. The curve shows the change in force when the cantilever is moved from the bulk towards the HOPG during push-in. The Y-axis indicates the force detected by the cantilever, and the X-axis indicates the position of the cantilever fixture, and not the position of the tip of the cantilever. Up to the 0 to −18 nm points on the horizontal axis, the position of the cantilever changes, but the value of the force does not change. This range is therefore considered to correspond to the bulk. When a cantilever is pushed into the ionic layer in a force curve measurement, the position where the slope of the graph finally becomes

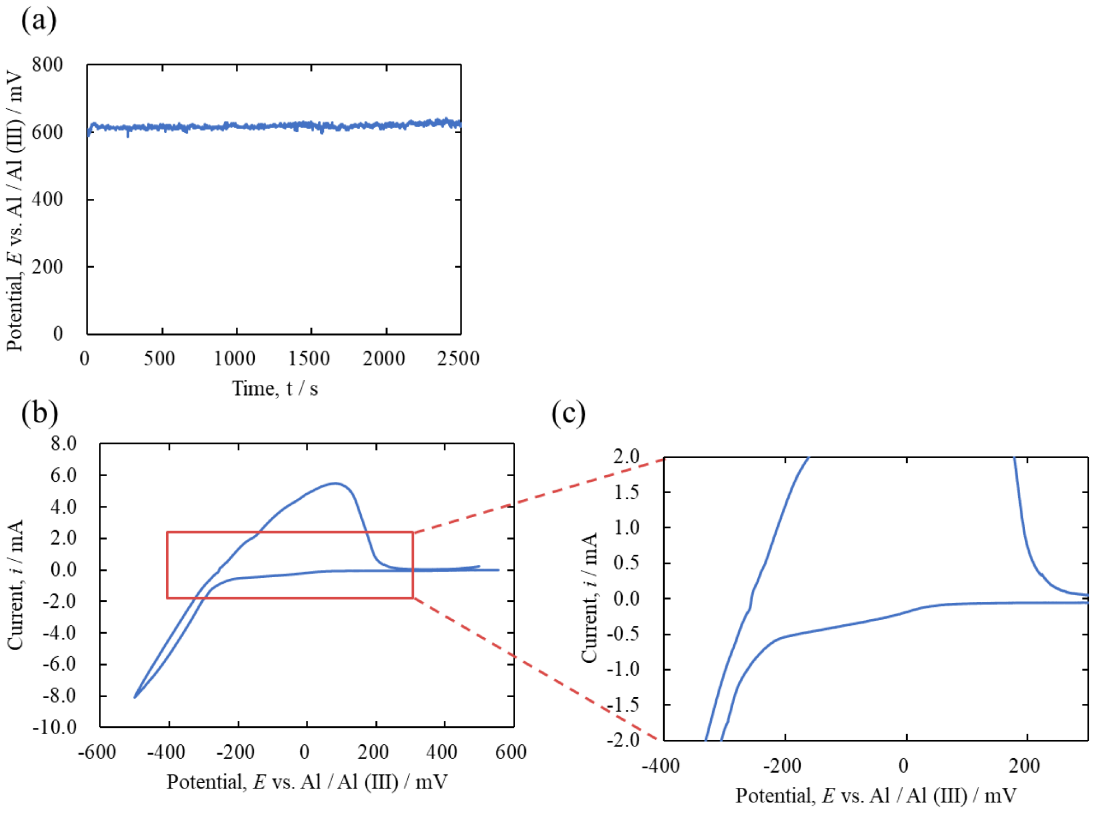

Figure 4. Electrochemical measurements in [EmIm][Al_2Cl_7] ionic liquid; (a) time variation of OCP of HOPG, (b) voltammogram measurement, (c) enlarged scale of the voltammogram.

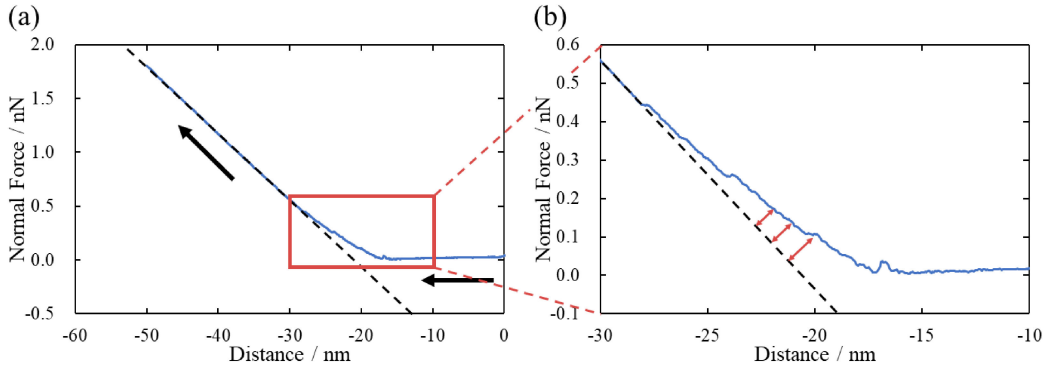

Figure 5. (a) Force curve during indentation on a HOPG electrode measured at OCP in [EmIm][Al_2Cl_7] ionic liquid and (b) an enlarged view of a part of Fig. 5a. (The position of the cantilever at the start of the measurement is set to 0.)

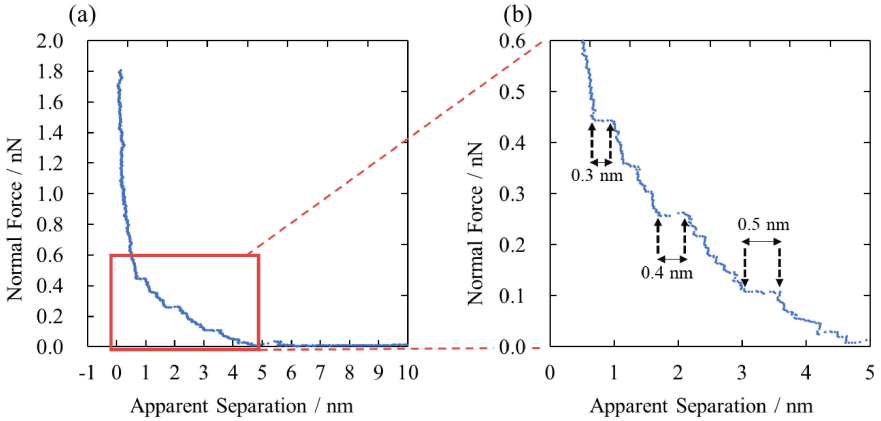

Figure 6. Transformed force curve of Fig. 5, (a) relation between normal force and apparent separation and (b) an enlarged view of a part of Fig. 6a.

constant is defined as the final arrival point of the tip of the cantilever. In this figure, the slope of the graph is constant in the range of −30 nm to −50 nm, so this position is considered to be the final arrival point. It has been reported that the cantilever cannot penetrate the strong ionic layer near the interface. Therefore, the final arrival point in this experiment is not on the HOPG plate, and is considered to be on the ionic layer that the cantilever could not penetrate.[14,27–29] Figure 6a shows the extrapolated line in the linear range from −30 nm to −50 nm in Fig. 5a, extended in the y-axis direction, and the difference between the extrapolated line (final arrival point) and the measured force curve indicated as distance. The distance from the final arrival point is showed by the double arrows in Fig. 5b. A magnified view of Fig. 6a is shown in Fig. 6b. In this figure, three obvious steps were observed before reaching the final arrival point. The width of each step was 0.3 nm, 0.4 nm, and 0.5 nm from the final arrival point.

If the needle tip of the cantilever cannot move deeper owing to the resistance of the ionic layer, the position of the cantilever will not change and the cantilever will be deflected. Therefore, in the normal part of the graph, it extends diagonally up to the left. When a certain amount of force is accumulated in the cantilever as deflection, the probe penetrates the ionic layer. At this point, the force applied to the cantilever does not change and it continues to move until it penetrates the ionic layer.

Unlike before that point on the graph, the x-axis value changes but the y-axis value does not. Therefore, a confirmed step appeared on the graph. The width of the step is not different compared to the results of the previous study, where the thickness of the $EmIm^+$ cation was 0.28 nm[30] and the thickness of the $Al_2Cl_7^-$ anion was 0.50 nm.[31] The force curve measurements of the present experiment, as in the previous study of Atkin et al.[14,15] allow us to measure the ionic layer.

In Fig. 6b, a slow change is observed between the ion layers, but this change is not a gap between the ion layers. This change is thought to be due to the force accumulated in the cantilever as deflection when the tip of the cantilever stops not being able to penetrate the ion layer. The force penetrating the ionic layer is considered to be stronger the closer it is to the electrode interface. Therefore, the deflection of the cantilever on the ionic layer near the electrode interface is closer to the deflection of the cantilever at the final arrival point than the deflection of the cantilever against the ionic layer near the bulk. This difference is the reason for the different slopes of the rising graphs after penetrating the ionic layer in Fig. 6b.

3.3 Force curve measurements under applying potential

Next, force curve measurements were obtained with potential applied to the electrochemical cell. The applied potential ranged from 0 to 710 mV; as in the OCP measurement, a step was observed near the final arrival point even with the potential applied. The thickness of the ionic layer and force required to penetrate the layer at each applied potential are shown in Fig. 7, with the layer closest to the final arrival point as the first layer and the layer following it as the second layer. The error ranges were calculated based on standard deviations. Figures 7a and 7b show that there was a significant difference in the force required to penetrate the ionic layer between the first and second layers. However, there was no difference in the force due to potential. The difference in the force required to

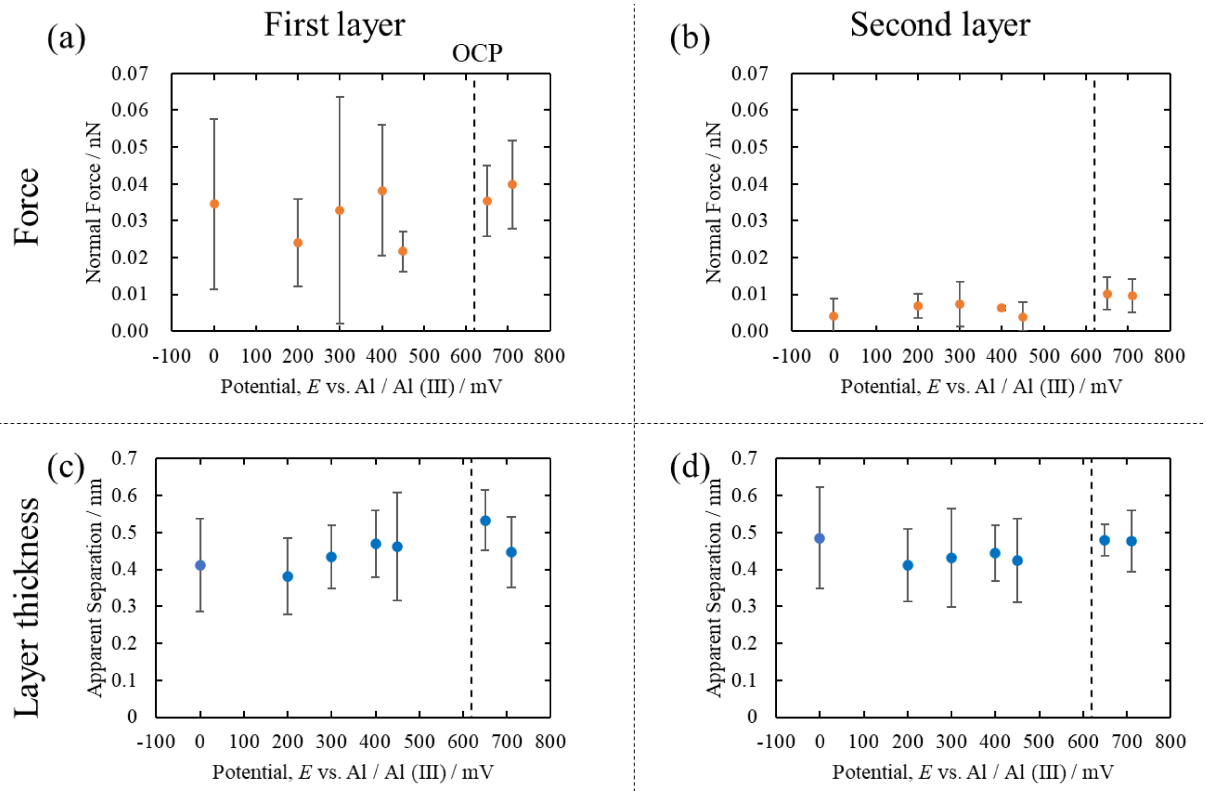

Figure 7. Results of force curve analysis under the applied potential; (a) potential change in the force required to penetrate the first layer, (b) potential change in the force required to penetrate the second layer, (c) potential change in the thickness of the first layer, (d) potential change in the thickness of the second layer.

penetrate shows that the first layer forms a stronger layer than the second layer.

A change in thickness of the first layer was observed with the applied potential, but not in the second layer. The formation of a strong layer is affected by the density and denseness of the ionic species within the ionic layer. Barbosa et al. reported the change in stiffness of the ionic layer with applied potential for 1-ethyl-3-methylimidazolium bis(trifluoromethylsulfonyl)imide ([EmIm][TFSI]) electric bilayer structures at a charged tungsten oxide interface.[32] Barbosa et al. stated that the increase in stiffness with applied potential is due to a change in the ionic orientation near the interface. He also reported that the stiffness of the ion layer was increased by the alignment of the ionic orientation angles owing to the applied potential. Moreover, it was considered that the stiffness of the ionic layer was increased by the increase in density of the ionic species due to the applied potential. The change in the force required to penetrate the first and second layers in this experiment may be due to the greater interaction between the ions in the ion layer because of the orientation angle of the ions. Because the first layer is closer to the interface than the second layer, it is also expected to affect the structure of the ionic layer closer to the interface.

Baldelli et al. reported that HOPG and $EmIm^+$ cations attract each other by π-π stacking.[15] This could facilitate the formation of regular structures of ionic liquids at the interface. The structure of the ionic layer that forms a regular structure at the interface affects the ionic layers that are formed next to it. The influence could decrease as one moves away from the interface, and it is deduced that as the ionic layer approaches the bulk, the orientation angles of the ions become more random. Therefore, the first layer closer to the interface has a more aligned ionic orientation angle than the second layer, making the first layer more difficult for the cantilever to penetrate than the second layer.

Figures 7c and 7d show that the thickness of the first layer changed with the potential, but not with the second layer. The thickness of the first layer decreased as one moved from the OCP to the lower potential side.

The decrease in the width of the ionic layer may be due to the attraction of ions near the bulk to the interface by the application of electricity. Because the ions are attracted to the interface, the ionic layer containing the ions is also attracted to the interface. As the ionic layer on the bulk side is attracted, the ionic layer on the interface side is subjected to compression from the ionic layer on the bulk side. The stronger compression reduces the degree of freedom of the ion array angle of the ion layer and reduces the randomness of the arrayed ions. Therefore, it is assumed that the applied potential biases the arrangement of the ionic species to a specific angle, resulting in the densification of the ionic layer and a decrease in the layer width. However, as shown in Figs. 7a and 7b, there was no predominant difference in the change in the force required to penetrate the ionic layer owing to the applied potential. It is deduced that near the bulk, even the potential right before electrodeposition would have changed only to the decrease in the layer width. Another possibility is that the ionic layer, which was measurable, may have formed so densely that it could not be penetrated by the cantilever owing to the applied potential.

If the formation of the dense layer is assumed to occur near the interface, it is likely that more ion attracting occurs near the interface, resulting in a reduction of the ion layer width. Assuming that this occurs while considering the structure of the ions at the interface, the following two mechanisms for the reduction of $Al_2Cl_7^-$ are expected. One is to assume a cation-dominated, negatively charged electrode interface as shown in Fig. 1. Here, the application of potential decreases the thickness of each ionic layer, bringing $Al_2Cl_7^-$ closer to the electrode, and providing electrons from the electrode to $Al_2Cl_7^-$ by the tunneling effect,

although $EmIm^+$ is present between them. The $Al_2Cl_7^-$ that receives the electrons is reduced to metal aluminum and is deposited on the electrode surface.

Second, the ionic layer near the interface is not completely a cationic layer, but anions are also present. Negatively charged electrode surfaces have a high amount of cations, but the possibility that anions may also be present has been reported in simulations of ionic liquids other than the present study. Shan Zhou et al. performed simulations in graphite and [EmIm][TFSI] ionic liquids.[33] In their simulations, they assumed that $TFSI^-$ anions are present in the first layer and that they are perpendicular to the electrode between the cations. Iwahashi et al. schematically modeled the interface between the Pt electrode and 1-ethyl-3-methylimidazolium bis(fluorosulfonyl)amide ([C_2mim][FSA]) from electrochemical measurements; when −1.0 V was applied to the Pt electrode, some FSA^- anions were present at the interface.[34] However, anions are likely to be present as part of the structure. A possible mechanism is when the $Al_2Cl_7^-$ anion receives electrons and aluminum deposition occurs.

4. Conclusions

The layers of ions present at the interface between HOPG and [EmIm][Al_2Cl_7] ionic liquid were evaluated using AFM force curve measurements with or without applied potential.

1. From the results of the force curve measurements, different ionic layer steps were observed at the interface between the [EmIm][Al_2Cl_7] ionic liquid and HOPG.
2. These steps were 0.3, 0.4, and 0.5 nm, and were considered to be arranged ionic layers.
3. In the [EmIm][Al_2Cl_7] ionic liquid, the thickness of the ionic layer decreased at the lower side when the force curve measurement was performed with a potential lower than that of the OCP. The thickness of the ionic layer decreased at the higher side when the force curve measurement was performed with a potential lower than that of the OCP.

Acknowledgments

This work was supported by a JSPS KAKENHI Grant Number 21K04734.

CRediT Authorship Contribution Statement

Atsuki Tabo: Formal analysis (Lead), Investigation (Lead), Writing – original draft (Equal)
Hisayoshi Matsushima: Conceptualization (Equal), Formal analysis (Equal)
Takahiro Ohkubo: Formal analysis (Equal), Software (Equal)
Kei Nishikawa: Formal analysis (Equal), Investigation (Supporting)
Mikito Ueda: Conceptualization (Lead), Investigation (Supporting), Project administration (Lead), Supervision (Lead), Writing – review & editing (Lead)

Conflict of Interest

The authors declare no conflict of interest in the manuscript.

Funding

Japan Society for the Promotion of Science: 21K04734

References

1. H. Liu, Y. Liu, and J. Li, *Phys. Chem. Chem. Phys.*, **12**, 1685 (2010).
2. A. P. Abbott and K. J. McKenzie, *Phys. Chem. Chem. Phys.*, **8**, 4265 (2006).
3. F. Endres, *Phys. Chem. Chem. Phys.*, **3**, 144 (2002).
4. I. Osada, H. de Vries, B. Scrosati, and S. Passerini, *Angew. Chem., Int. Ed.*, **55**, 500 (2016).
5. A. Lewandowski and A. Swiderska-Mocek, *J. Power Sources*, **194**, 601 (2009).
6. D. M. Kolb, *Angew. Chem., Int. Ed.*, **40**, 1162 (2001).
7. M. V. Fedorov, N. Georgi, and A. A. Kornyshev, *Electrochem. Commun.*, **12**, 296 (2010).
8. M. Mezger, H. Schröder, H. Reichert, S. Schramm, J. S. Okasinski, S. Schöder, V. Honkimäki, M. Deutsch, B. M. Ocko, J. Ralston, M. Rohwerder, M. Stratmann, and H. Dosch, *Science*, **322**, 424 (2008).
9. M. Z. Bazant, B. D. Storey, and A. A. Kornyshev, *Phys. Rev. Lett.*, **106**, 046102 (2011).
10. V. Ivaništšev, S. O'Connor, and M. V. Fedorov, *Electrochem. Commun.*, **48**, 61 (2014).
11. S. Baldelli, *Acc. Chem. Res.*, **41**, 421 (2008).
12. F. Endres, N. Borisenko, S. Z. el Abedin, R. Hayes, and R. Atkin, *Faraday Discuss.*, **154**, 221 (2012).
13. K. Fukui, *Bull. Chem. Soc. Jpn.*, **91**, 1210 (2018).
14. R. Hayes, N. Borisenko, M. K. Tam, P. C. Howlett, F. Endres, and R. Atkin, *J. Phys. Chem. C*, **115**, 6855 (2011).
15. T. Carstens, R. Gustus, O. Höfft, N. Borisenko, F. Endres, H. Li, R. J. Wood, A. J. Page, and R. Atkin, *J. Phys. Chem. C*, **118**, 10833 (2014).
16. Y. Yokota, H. Hara, Y. Morino, K. Bando, A. Imanishi, T. Uemura, J. Takeya, and K. Fukui, *Phys. Chem. Chem. Phys.*, **17**, 6794 (2015).
17. P. Simon and Y. Gogotsi, *Nat. Mater.*, **19**, 1151 (2020).
18. Y. He, H. Li, C. Qu, W. Cao, and M. Ma, *Green Chem. Eng.*, **2**, 145 (2021).
19. Y.-X. Zhong, J.-W. Yan, M.-G. Li, X. Zhang, D.-W. He, and B.-W. Mao, *J. Am. Chem. Soc.*, **136**, 14682 (2014).
20. T. Cui, A. Lahiri, T. Carstens, N. Borisenko, G. Pulletikurthi, C. Kuhl, and F. Endres, *J. Phys. Chem. C*, **120**, 9341 (2016).
21. L. A. Jurado and R. M. Espinosa-Marzal, *Sci. Rep.*, **7**, 4225 (2017).
22. A. P. Abbott, G. Frisch, and K. S. Ryder, *Annu. Rev. Mater. Res.*, **43**, 335 (2013).
23. L. Sun and J. F. Brennecke, *Ind. Eng. Chem. Res.*, **54**, 4879 (2015).
24. S. Takahashi, K. Akimoto, and I. Saeki, *Surf. Technol.*, **40**, 548 (1989).
25. R. J. Gale and R. A. Osteryoung, *Inorg. Chem.*, **18**, 1603 (1979).
26. M. J. Frisch, G. W. Trucks, H. B. Schlegel, G. E. Scuseria, M. A. Robb, J. R. Cheeseman, G. Scal-mani, V. Barone, G. A. Petersson, H. Nakatsuji, X. Li, M. Caricato, A. V. Marenich, J. Bloino, B. G. Janesko, R. Gomperts, B. Mennucci, H. P. Hratchian, J. V. Ortiz, A. F. Izmaylov, J. L. Sonnenberg, D. Williams-Young, F. Ding, F. Lipparini, F. Egidi, J. Goings, B. Peng, A. Petrone, T. Henderson, D. Ranasinghe, V. G. Zakrzewski, J. Gao, N. Rega, G. Zheng, W. Liang, M. Hada, M. Ehara, K. Toyota, R. Fukuda, J. Hasegawa, M. Ishida, T. Nakajima, Y. Honda, O. Kitao, H. Nakai, T. Vreven, K. Throssell, J. A. Montgomery, Jr., J. E. Peralta, F. Ogliaro, M. J. Bearpark, J. J. Heyd, E. N. Brothers, K. N. Kudin, V. N. Staroverov, T. A. Keith, R. Kobayashi, J. Normand, K. Raghavachari, A. P. Ren-dell, J. C. Burant, S. S. Iyengar, J. Tomasi, M. Cossi, J. M. Millam, M. Klene, C. Adamo, R. Cammi, J. W. Ochterski, R. L. Martin, K. Morokuma, O. Farkas, J. B. Foresman, and D. J. Fox, Gaussian, Inc., Wallingford CT (2016).
27. H. Li, F. Endresb, and R. Atkin, *Phys. Chem. Chem. Phys.*, **15**, 14624 (2013).
28. J. Sweeney, F. Hausen, R. Hayes, G. B. Webber, F. Endres, M. W. Rutland, R. Bennewitz, and R. Atkin, *Phys. Rev. Lett.*, **109**, 155502 (2012).
29. H. Li, M. W. Rutlandbc, and R. Atkin, *Phys. Chem. Chem. Phys.*, **15**, 14616 (2013).
30. A. Elbourne, S. McDonald, K. Voïchovsky, F. Endres, G. G. Warr, and R. Atkin, *ACS Nano*, **9**, 7608 (2015).
31. H. Li, Y. Chang, W. Zhu, W. Jiang, M. Zhang, J. Xia, S. Yin, and H. Li, *J. Phys. Chem.*, **119**, 5995 (2015).
32. M. S. Barbosa, N. Balke, W.-Y. Tsai, C. Santato, and M. O. Orlandi, *J. Phys. Chem. Lett.*, **11**, 3257 (2020).
33. S. Zhou, K. S. Panse, M. H. Motevaselian, N. R. Aluru, and Y. Zhang, *ACS Nano*, **14**, 17515 (2020).
34. T. Iwahashi, Y. Miwa, W. Zhou, Y. Sakai, M. Yamagata, M. Ishikawa, D. Kim, and Y. Ouchi, *Electrochem. Commun.*, **72**, 54 (2016).